Flux-creep studies of vortex pinning in an aligned $YBa_2Cu_3O_{7-\delta}$ superconductor with oxygen deficiencies $\delta \leq 0.2$

J. G. Ossandon
Department of Physics, University of Tennessee, Knoxville Tennessee 37996-1200

J. R. Thompson
Solid State Division, Oak Ridge National Laboratory, Building 3115, P.O. Box 2008, Oak Ridge, Tennessee 37831-6061 and Department of Physics, University of Tennessee, Knoxville, Tennessee 37996-1200

D. K. Christen and B. C. Sales
Solid State Division, Oak Ridge National Laboratory, Building 3115, P.O. Box 2008, Oak Ridge, Tennessee 37831-6061

Yangren Sun
Department of Physics, University of Tennessee, Knoxville Tennessee 37996-1200

K. W. Lay
General Electric Corporate Research and Development Center, Schenectady, New York 12301
(Received 5 March 1992)

Flux-creep measurements were carried out in magnetically aligned, sintered samples of $YBa_2Cu_3O_{7-\delta}$ with various oxygen deficiencies δ (in the range $0 \leq \delta \leq 0.2$), for temperatures T in the range from 5 to 75 K, with an applied magnetic field $\mathbf{H} \| c$ axis of 1 T. The normalized flux-creep rate $S = d \ln M / d \ln t$ was determined as a function of T and δ. The effective vortex-pinning potential $U_{\text{eff}}(J)$ and the pinning energy U_0 were calculated both in the linear Anderson-Kim approximation as well as in the nonlinear formalism of vortex-glass and collective-pinning theory. The applicability of the nonlinear formalism was tested and discussed. There is a close correspondence between the energy scaling parameter U_0 of the nonlinear model and the pinning energy of a pointlike pinning center. A comparison of the experimental results with predictions of collective-pinning theory reveals a consistent picture of vortex motion in this family of superconductors.

I. INTRODUCTION

A recent systematic study[1] of the influence of oxygen deficiency δ (for $0 \leq \delta \leq 0.2$) on the magnetic superconducting properties of grain-aligned, sintered samples of $YBa_2Cu_2O_{7-\delta}$ has shown that a relatively small oxygen deficiency strongly reduces the condensation energy $F_c = H_c^2/8\pi$ of the material, with a consequent decrease of the critical current density J_c and the associated pinning of vortices. The present paper describes a flux-creep investigation conducted on the same samples in order to study the effects of small oxygen deficiencies on the magnetic relaxation and/or flux-creep properties of this material. These results constitute a test case for recent theory of collective flux creep and have, in addition, significant practical implications for potential applications of $YBa_2Cu_3O_{7-\delta}$ materials.

II. EXPERIMENTAL ASPECTS

The sample synthesis and characterization have been described in detail elsewhere.[1,2] Briefly described, an aligned polycrystalline mass was formed using a 4 T magnetic field to align previously synthesized single crystallites of YBCO; the particles were suspended in an organic liquid that subsequently evaporated. The grains were sintered together at an elevated temperature to form a porous but mechanically stable sample. The individual crystallites in the resulting sample were aligned with their c axes oriented within a rocking curve FWHM of 7°, as determined by x-ray diffraction. The sample shape was cubic, of approximate dimensions $3 \times 3 \times 3$ mm^3, with one face perpendicular to the c-orientation. The oxygen content $x = 7 - \delta$ was established using a Thermogravimetric Analysis system and was determined *in situ* by the same apparatus. Five oxygen compositions were investigated, namely, $x = 7.00$ (defined as the fully oxygenated sample), $x = 6.94$, 6.89, 6.85, and 6.80. The small grain size, $\sim 7\mu$m, and open, relatively porous structure with 78% of theoretical density allowed rapid, uniform, and reproducible adjustment of the "chain-site" oxygen content.

The magnetic relaxation measurements were carried out in a SQUID magnetometer (Quantum Design Inc. model MPMS). It was operated in a "no overshoot" mode for the magnetic field, with a scan length of 2 cm to minimize effects of field inhomogeneities. The sample was mounted on a quartz disk with c axis oriented along the field direction. For each oxygen composition, magnetization versus time profiles were determined at the following fixed temperatures: 5, 7, 10, 15, 20, 30, 40, 50, 60, 70, and 75 K. Before measurements at each temperature,

the sample was made virgin by turning off the applied field and heating to $T=110$ K for 15 min. It was then cooled in zero field and stabilized at the desired temperature for 30 min, after which a field of 1 T was applied parallel to the c axis of the sample. Measurements of magnetization versus time started about 1 min after the magnetic field was applied. Each data set, corresponding to a particular temperature setting, consisted of 21 data points separated by an increasing time interval, for a total time span of 4.5 h. Complementary measurements of magnetic hysteresis loops were made with a vibrating sample magnetometer (VSM) under swept field conditions. In the present study, these data were used to determine both the equilibrium superconductive magnetization for correction purposes and the "initial" magnetization, as described below.

To obtain the hysteretic component of magnetization that is proportional to the circulating current density J, the equilibrium magnetization must be subtracted from the measured value. We used the following procedure. First, the measured magnetic moment $m(t)$ was corrected for the paramagnetic background of the quartz disk by extrapolating measurements from high temperature $T \geq T_c$, assuming a Curie-Weiss temperature dependence. Next, values of the reversible (equilibrium) magnetization $M_{\rm rev}$ were obtained from VSM hysteresis loops $M(H)$ measured up to 6.5 T, by averaging the increasing field magnetization M^+ and the decreasing field magnetization M^- observed at $H=1$ T. This allowed calculation of the irreversible magnetization $M_{\rm irr}(t) \equiv M^+(t) - M_{\rm rev}$ associated with circulating critical currents.

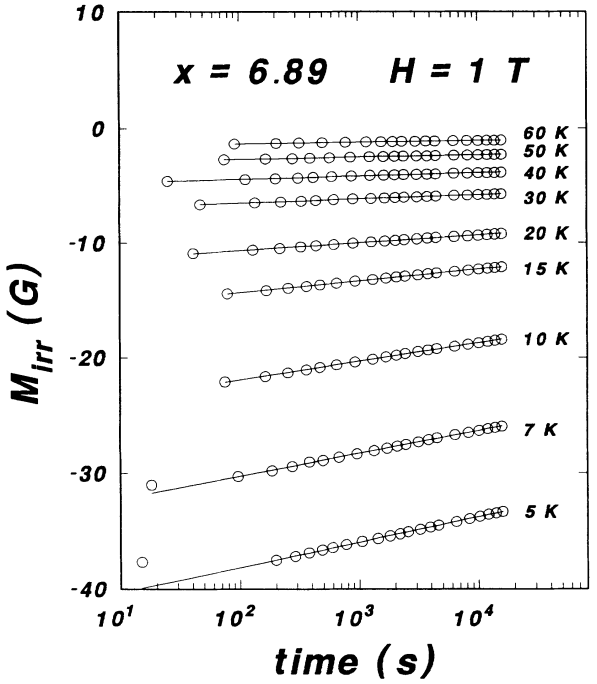

FIG. 1. Semilogarithmic plot of irreversible magnetization vs time illustrates the approximately logarithmic decay at the temperatures shown, for $YBa_2Cu_3O_x$, with $x=6.89$. Similar results were obtained for other oxygen compositions. Linear regression fits give the solid lines whose slopes are proportional to the "flux-creep rate" $S(T)$.

III. EXPERIMENTAL RESULTS AND ANALYSIS

To first order, the induced signal $M_{\rm irr}$ varied with the logarithm of time for all flux-creep measurements within the time span investigated. Linear regression analysis of the data $M_{\rm irr} \propto \ln(t)$ produced regression "goodness-of-fit" coefficients ρ^2 near 0.999. For each measurement, the problematical "origin" of time was adjusted slightly so as to maximize ρ^2. To minimize the influence of this problem, we excluded the initial one or two data points from the regression, which are the most sensitive to the exact choice of the time origin. Figure 1 shows typical results for $M_{\rm irr}$ vs t at different temperatures for one oxygen composition, where the solid lines are linear regression fits. Hereafter, the symbol M denotes the irreversible magnetization $M_{\rm irr}$ unless otherwise indicated.

We consider first the normalized flux-creep rate

$$S(t) \equiv |d \ln M / d \ln t| = |(1/M) dM / d \ln t| \propto |M^{-1}| , \quad (1)$$

which is defined so as to be positive in sign This quantity is slightly time dependent (since the magnitude of M slightly decreases in time). However, on the time scale of our measurements, it is well approximated by

$$S(t) = |(1/M_i) dM / d \ln t| , \quad (2)$$

where M_i is an appropriate "initial" value of the irreversible magnetization. We have chosen for M_i the dynamic irreversible magnetization measured in VSM hysteresis loops with $H=1$ T and increasing with a sweep rate of 10.8 mT/s. Values of $S(T)$ were determined at different temperatures and are plotted in Fig. 2 for the five oxygen compositions. They all center about a mean value of ≈ 0.02. An interesting feature of the $S(T)$ profiles is the peak at low temperatures, between 5 and 20 K. Most prominent in the case of the fully oxygenated sample, the peak decreases in magnitude as the oxygen deficiency increases, so that it almost fully disappears at $\delta=0.20$. Following the peak region, there is a plateau[3] in all five

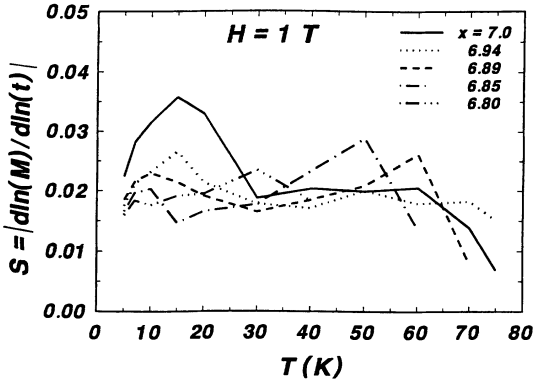

FIG. 2. Normalized flux-creep rate $S(T)$ vs temperature T for five oxygen compositions. The average height of the plateau, $S \approx 0.02$, is independent of δ.

$S(T)$ profiles, which extends over a temperature interval of 30–50 kelvins, depending on the sample. The position of the $S(T)$ plateau shifts along the T axis to lower temperatures as δ increases, but interestingly its average "height" of about 0.02 does not change and is independent of oxygen deficiency. Finally, at higher temperatures, there is some indication that the curves turn downward as they approach T_c, but these results are derived from rather small signals and are less reliable than those at lower temperatures.

In the following analysis, the effective potential $U_{\rm eff}(J)$ and the activation energy U_0 are analyzed using both the linear Anderson-Kim approximation and the nonlinear formalism of vortex-glass and collective-pinning theories. We consider first the older, linear theory. In the traditional Anderson-Kim theory of flux creep[4,5] for a superconductor in the critical state, the rate at which flux bundles jump over the pinning barriers due to thermal activation is given by an Arrhenius expression:

$$f = f_0 \exp\{-U_{\rm eff}/k_B T\} , \tag{3}$$

where f_0 is a characteristic "attempt frequency" (typically of the order of 10^{10}–10^{12} Hz). Now, $U_{\rm eff}$ must be a decreasing function of the driving Lorentz force $|F| = JB$ acting on the flux bundles. The simplest functional form (assuming a "sawtooth" pinning potential) is the linear relation

$$U_{\rm eff} = U_0^* - JBVX , \tag{4}$$

where U_0^* is the (Anderson-Kim) activation energy, V is the activation volume, and X is an effective pinning length. In this model $U_{\rm eff}$ and the current density J are linearly related. Assuming $J \approx J_c$ (critical state) and using the linear approximation, Anderson and Kim solved the flux-creep equation in lowest order and found a logarithmic time decay of the "persistent" current:

$$J_c(t,T) = J_{c0}(T)[1-(k_B T/U_0^*)\ln(t/t_0)] . \tag{5}$$

Here J_{c0} is the critical current density in the absence of flux creep and t_0 ($\propto f_0^{-1}$) is a microscopic attempt time for hopping of a vortex or a bundle of vortices. Using the Bean model[6] to relate J_c to the irreversible magnetization M, the relaxation of the magnetization follows a similar logarithmic decay:

$$M(t) = M_0[1-(k_B T/U_0^*)\ln(t/t_0)] . \tag{6}$$

In this approximation, the logarithmic derivative of $M(t)$ is a constant, from which the activation energy U_0^* is determined in first approximation:

$$U_0^* = k_B T M_0/(dM/d\ln t) = k_B T/S , \tag{7}$$

where we used Eq. (2) with $M_i = M_0$. The resulting values of U_0^* are shown in Fig. 3 for the five oxygen compositions at various temperatures with a field of 1 T. Observe that the Anderson-Kim activation energy U_0^* has a value of about 20 meV (= 230 K) at 5 K and it increases steadily with T in all five cases, reflecting the relative constancy of $S(T)$.

It has become clear,[7,8] however, that the linear approximation does not adequately describe pinning in high-temperature superconductors. A more realistic approach incorporates a nonlinear relationship between $U_{\rm eff}$ and J, as discussed below. First we reanalyze the time-dependent magnetization to obtain model-independent experimental information on the temperature and J dependence of the pinning energy.

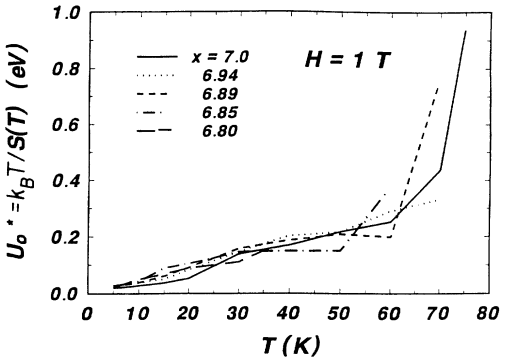

FIG. 3. The activation energy U_0^* in the (Anderson-Kim) linear model has a value of ≈ 25 meV at $T = 5$ K for all oxygen contents and increases steadily with T, reflecting the behavior of $S(T)$. As $T \to T_c$, however, U_0^* must vanish.

As described by Maley *et al.*,[9] we start with the relaxation rate equation that contains an Arrhenius factor, similar to Eq. (3):

$$dM/dt = (B\omega a/2\pi R)\exp(-U_{\rm eff}/k_B T) . \tag{8}$$

Here B is the flux density, $\omega/2\pi$ is an attempt frequency for vortex hopping, a is the hopping distance, and R is the sample radius. In general, the effective pinning potential $U_{\rm eff}$ is a function of J, T, and B. By inverting Eq. (8), $U_{\rm eff}$ can be expressed in the form

$$U_{\rm eff} = k_B T[\ln(dM/dt) - C] \quad \text{with } C = \ln(B\omega a/2\pi R) . \tag{9}$$

Hereafter we set $k_B = 1$ and count $U_{\rm eff}$ in temperature units (K).

The J dependency of $U_{\rm eff}$ in Eq. (9) can be made explicit by means of the Bean model. In our grain-aligned samples, the grain morphology can be approximated by a spherical shape, so that the Bean formula in this case[10] is

$$J_c = 16.9[\Delta M\ (\text{G})]/[R\ (\text{cm})]\ \text{A/cm}^2 . \tag{10}$$

In this expression we have $\Delta M \equiv M^+ - M^- = 2M = 2(M^+ - M_{\rm rev})$, with M in units of G and the grain radius R in centimeters.

Using Eqs. (9) and (10), separate segments of the curve $U_{\rm eff}(J,T)$ were obtained for each fixed temperature setting. At sufficiently low temperatures with a fixed applied field, the unknown factor C appearing in Eq. (9) can be considered constant since all intrinsic thermal factors, e.g., the condensation energy, coherence lengths, etc., that could influence ω and a, are nearly constant. With this assumption, the best value of C was chosen to make the separate portions of the $U_{\rm eff}(J,T)$ curves at low temperatures (from 5 to 15 K) fall on a smooth, continuous

function of J. Table I lists the optimum value of C for each oxygen composition.

The experimental curves $U_{\rm eff}(J,T)$ obtained in this manner are depicted in Fig. 4 for all five oxygen compositions at $T \leq 30$ K. Each segment corresponds to a series of ~ 21 data points, which are the same as those included in Fig. 1, for example. From the perspective of an Anderson-Kim analysis, we note that a linear projection of each data segment toward lower J values cuts the vertical axis ($J=0$) at a point equal to U_0^*. Observe that, for the 5-K segments of the five curves, the intersections of these linear projections are nearly the same, independent of oxygen content; this is consistent with the values shown in Fig. 3. Furthermore, different segments of the same curve have vertical intercepts that rise as T increases. This explains the strong temperature dependence of U_0^*.

With increasing temperature, the pinning potential weakens since the quantities on which it depends, e.g., the condensation energy, decrease and eventually go to zero at $T_c(B)$. This weakened potential is evident in the fact that, at higher temperatures, the separated portions of the curve (or individual sets of data) lie progressively below any reasonable extrapolation of the low temperature, smooth curve. There is no common, constant value of C that aligns all the segments on the same continuous function.

In order to extract a more accurate dependence $U_{\rm eff}(J,0)$ on current density as $T \rightarrow 0$, we must separate out this thermal dependence. We assume[11,12] that the temperature dependence of $U_{\rm eff}(J,T)$ can be described, in a first approximation, by a temperature function

$$g(T/T_x)=[1-(T/T_x)^2]^{3/2} \tag{11}$$

such that $U_{\rm eff}(J,T)$ can be written in the form

$$U_{\rm eff}(J,T)=g(T/T_x)U_{\rm eff}(J,0) \ . \tag{12}$$

The function $g(T/T_x)$ approximates the temperature dependence of the pinning potential expected classically, where T_x is the transition temperature. We use values of T_x at $H=1$ T from the corresponding $H_{c2}(T)$ lines established for the same sample and oxygen compositions in a previous work.[1] These values differ little from other measures of T_c and the end results are relatively insensitive to the exact value selected for T_x, except near the superconductive transition.

Having chosen a value of C to align the low-temperature segments of the curve, we use that value at all temperatures to obtain $U(J,T)$. Dividing this quantity by $g(T/T_x)$ gives $U_{\rm eff}(J,0)$. As an example, Fig. 5 shows both $U_{\rm eff}(J,T)$ and $U_{\rm eff}(J,0)$ for the fully oxygenated sample ($x=7.0$). Observe that these two functions coincide quite well at low temperature, but they separate progressively for $T \geq 20$ K. The symbols in Fig. 5 represent the experimental, highly nonlinear relation between $U_{\rm eff}$ and J.

The solid line in Fig. 5 is a theoretical form for $U_{\rm eff}(J,0)$ provided by vortex-glass[13] and collective-pinning theories,[14–16] which have been fitted to the experimental data. Both theoretical treatments lead to a J-

TABLE I. Optimum parameter values for various oxygen contents ($\mathbf{H}\|c, H=1$ T).

Oxygen content x	7.00	6.94	6.89	6.85	6.80
T_{cx} (K)	88.5	89.7	86.9	77.7	65.4
$T_{\rm irr}$ (K)	87.0	85.7	83.2	73.5	61.0
C	15	16.5	17.4	17.5	18
μ	0.82	0.91	0.90	0.95	0.95
J_{c0} (MA/cm^2)	9.0	6.0	5.1	3.4	2.4
U_0 (K)	91	90	67	64	73

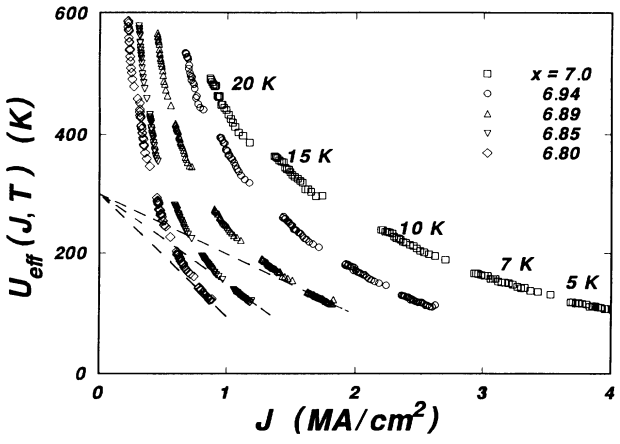

FIG. 4. Experimental results for $U_{\rm eff}(J,T)$ vs $J(T)$ at fixed low temperatures T for each oxygen composition. See text and Eq. (9) for analysis method that aligns segments to form a smooth function. Each segment contains the same series of ≈ 21 points as in Fig. 1. Note that a linear projection of each segment toward $J=0$ cuts the vertical axis at the value $U_0^*(T,\delta)$. This explains the strong temperature dependence of U_0^*.

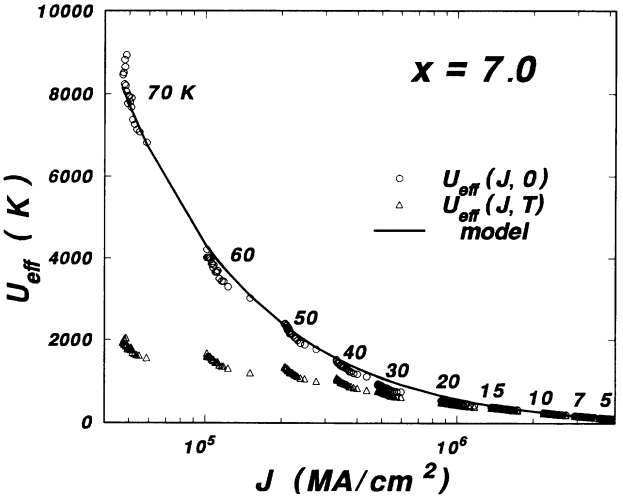

FIG. 5. Progressive separation between $U_{\rm eff}(J,T)$ and $U_{\rm eff}(J,0)$, as generated by the temperature function $g(T/T_x)$ [Eq. (11)] for one oxygen content ($x=7.0$). The solid line is a theoretical fit to results from vortex-glass collective-pinning theories.

dependent $U_{\rm eff}$ of the form

$$U_{\rm eff}(J,0)=(U_0/\mu)[(J_{c0}/J)^{\mu}-1]\ , \tag{13}$$

where μ is a dimensionless exponent that may depend on field and temperature, J_{c0} is the zero-temperature critical current density in the absence of flux creep, and U_0 sets an energy scale whose precise meaning will be discussed in a later section. This expression leads to an "interpolation" formula for the time-dependent magnetization

$$M(t)=M_0/[1+(\mu k_B T/U_0)\ln(t/t_{\rm eff})]^{1/\mu}\ , \tag{14}$$

where $t_{\rm eff}$ is a macroscopic, effective time scale. This interpolation formula has provided an accurate description of long-term studies[17] of magnetic relaxation (up to $\sim$4 days duration) in proton-irradiated YBCO single crystals. The expression successfully characterized the nonlogarithmic time dependence of $M(t)$.

One of the main objectives in this study was to test the applicability of Eq. (13) and to determine the optimum values of the parameters μ, J_{c0}, and U_0 for all five oxygen compositions. In Fig. 6 are shown experimental results for $U_{\rm eff}(J,0)$ at low temperatures (5–20 K) with solid lines corresponding to optimum fits to Eq. (13). The resulting values for the parameters are tabulated in Table I. A logarithmic axis for the independent variable J was used in this figure and only low-temperature portions of the curves are shown. In earlier transport studies on thin YBCO films, Zeldov *et al.*[18] observed a dependence on J of the form $U_{\rm eff}(J)\propto\ln(J)$. On the other hand, our results for $U_{\rm eff}(J)$ vs $\ln(J)$ persistently curve upward, even at the lowest U values measured. The overall behavior for experiments up to 70 K is shown in Fig. 7. Both axes of this figure use logarithmic scales due to the pronounced upward curvature of the function $U_{\rm eff}(J,0)$ as $J(T)$ decreases.

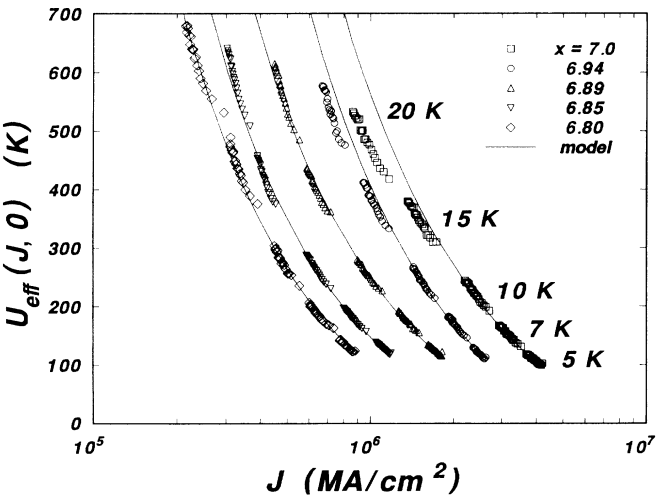

FIG. 6. Pinning potential $U_{\rm eff}$ vs J, at low temperatures. Solid lines are fits to the nonlinear potential, Eq. (13), using parameter values in Table I. Analytical extrapolations of the lines to $U_{\rm eff}\to 0$ intercept the horizontal axis at the points $J_{c0}(\delta)$, given in Table I.

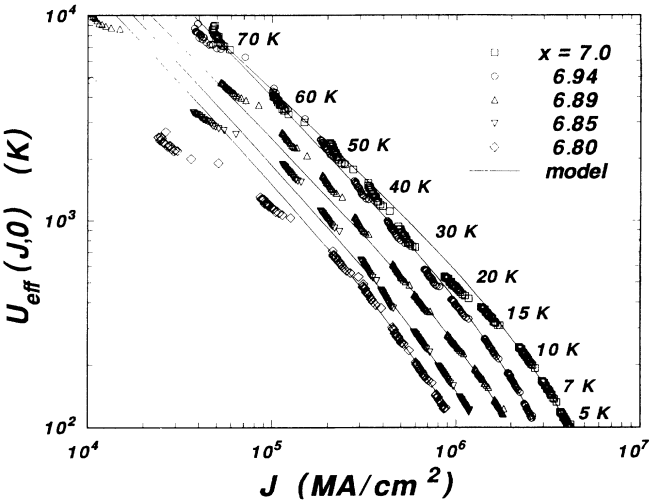

FIG. 7. A log-log plot of U vs J including data from all temperatures. The model potential gives a good description of the experimental results for the samples with higher oxygen content. At high temperatures, the description is less satisfactory for the lowest oxygen stoichiometries. The agreement can be improved if the transition temperature T_{cx} (from the H_{c2} line) is replaced (somewhat artificially) by the temperature $T_{\rm irr}(H)$ of the irreversibility line.

IV. DISCUSSION

From observation of Fig. 7 we conclude that, for the samples with highest oxygen content ($x=7.00$ and 6.94), the effective potential model [Eq. (13)] gives a fairly good description of the experimental data in the whole temperature range (5–70 K). However, for the samples with lower oxygen content, the theoretical function agrees well with the data only up to 60 K (for $x=6.89$); up to 40 K (for $x=6.85$), and up to 20 K (for $x=6.80$). At temperatures above these thresholds, the experimental points separate progressively from the solid lines, i.e., the curves $U_{\rm eff}(J,0)$ bent down faster than predicted by Eq. (13). This means that in these samples the temperature dependency of $U_{\rm eff}(J,T)$ is stronger than expected. One possible explanation is that the relevant transition temperature T_x in Eq. (11) is lower than that obtained from the $H_{c2}(T)$ line. Indeed, it has been argued by Maley *et al.*[11] that T_x is more nearly the temperature $T_{\rm irr}(H)$ of the irreversibility line in field H. We have tested this proposition and find that it considerably improves the fit at higher temperatures, while there is no significant change at lower temperatures. In a previous study,[1] values of $T_{\rm irr}$ at $H=1$ T were determined for the different oxygen concentrations and are given for the record in Table I. The choice of $T_{\rm irr}$, instead of $T(H_{c2})$, as the relevant transition temperature is more significant in the oxygen-depleted samples, since $T_{\rm irr}$ lies progressively far below $T(H_{c2})$ as δ increases. However, we question the validity of using $T_{\rm irr}$ in this analysis, so all results presented here were obtained using $T_x=T(H_{c2})$. In any event, the remaining parameters in Table I (C, U_0, J_{c0}, and μ) are not affected by the choice of T_x since they were extracted

from the low-temperature portions of the $U(J)$ curves.

The exponent μ is practically independent of oxygen stoichiometry δ, with a value of ≈ 0.9. This result is well within the theoretical bound ($\mu \leq 1$) of the vortex-glass model, as well as the maximum of $\frac{3}{2}$ allowed by the collective-pinning model. The validity of this value, $\mu \approx 0.9$, has been substantiated by a more detailed analysis of the time dependence of $M(t)$, using the interpolation formula, Eq. (14). Analysis of the explicit time dependence yielded μ values in the range 0.85–1.0 for all compositions at all temperatures $T \leq 40$ K where the data were sufficiently precise for the analysis. Relative to the Kim-Anderson expression, Eq. (6), linear regressions to the interpolation formula [Eq. (14)] were superior, as evidenced by larger "goodness-of-fit" regression coefficients ρ^2.

The additive parameter C increases slightly with δ, from $C \approx 15$ for $\delta = 0$ to $C \approx 18$ for $\delta = 0.2$. From its definition in Eq. (9), we conclude that the product ωa has been amplified by a factor of ≈ 20 as oxygen was removed from the chain sites. Either the attempt frequency ω or the hopping distance a, or both, experience an increase with δ. An interpretation of this result has not yet been elaborated.

The critical current density in the absence of flux creep J_{c0} decays strongly with increasing δ, as expected. From studies of the equilibrium magnetization, it has been established[1] that, in $YBa_2Cu_3O_{7-\delta}$, the extrapolated condensation energy $F_c = H_c^2/8\pi$ at $T = 0$ decreases sharply from 0.45 to 0.036 J/cm^3 ($\pm 10\%$) as δ changes from 0 to 0.2, respectively. This has a direct, negative impact on the quantity $F_c(0)\xi_{ab}(0)$, which we denote as the "pinning parameter." Explicitly, this quantity is proportional to the elementary pinning force per unit length of vortex core that resides in a pinning site. Earlier we have presented evidence that the strong pinning centers in these $YBa_2Cu_3O_{7-\delta}$ materials are not oxygen vacancies but are rather preexisting pointlike defects. Figure 8 compares the values of $J_{c0}(\delta)$ obtained here with values for the pinning parameter, for each oxygen composition. These quantities, which are directly proportional according to a simple, single-site pinning model,[1] are relatively well correlated experimentally. It is significant that the values for J_{c0} are obtained from an analysis of time-dependent, *irreversible* magnetization, while values for the pinning parameter come from studies of the *equilibrium* superconductive properties of the same materials.

Finally, from Table I we observe a somewhat curious variation of the energy U_0 with composition δ. Initially $U_0(\delta)$ decreases as δ goes from 0 to 0.15, but then it increases for $\delta = 0.2$. Since experimental studies show that the condensation energy F_c drops sharply with δ and that the density of strong pinning centers is practically constant,[1] how is it that U_0 varies so little in the range $0 \leq \delta \leq 0.2$?

An interpretation of this result can be obtained within a single-site pinning model. Such individual pinning sites can arise from site-antisite defects, vacancies, and interstitial atoms that are incorporated in the crystalline lattice during materials synthesis. Similar pinning sites can also be created in large numbers by irradiation with light ions such as protons.[19]

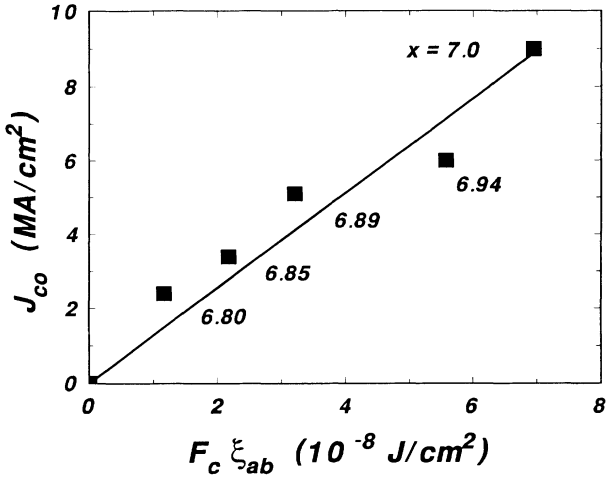

FIG. 8. The values of $J_{c0}(T=0)$ and the product $F_c(0)\xi_{ab}(0)$, obtained with different oxygen contents, are fairly well correlated. The line is a linear regression with zero intercept.

Consider a pointlike pin with pinning energy

$$E_{\text{pin}} \propto F_c \pi \xi_{ab}^2 \xi_c \ , \tag{15}$$

where F_c (condensation energy density) represents the pinning energy per unit volume, and $\pi\xi_{ab}^2\xi_c$ is proportional to the volume of flux core that is effectively pinned. We assume throughout that the temperature is constant. Since $\xi_c = \xi_{ab}/\gamma$, where $\gamma = (m_3/m_1)^{1/2}$ is the superconducting mass anisotropy parameter, it follows that the pinning energy E_{pin} according to this simple model must be proportional to the product $F_c(\pi/\gamma)\xi_{ab}^3$. The variation of E_{pin} with oxygen stoichiometry depends not only on $F_c(\delta)$, but also on the dependencies of $\gamma(\delta)$ and $\xi_{ab}^3(\delta)$ on δ.

We use again results from our previous work[1] to test this proposition. In that work, the parameter γ was found to be ≈ 5.4 and independent of δ in the range $0 \leq \delta \leq 0.2$, while the coherence length ξ_{ab} increased with δ. Consequently, the volume of the pinned vortex core should expand significantly with increasing δ, thereby counteracting the sharp decay of F_c. In Fig. 9 is plotted, in units of meV, both the product $F_c(\pi/\gamma)\xi_{ab}^3$ evaluated at $T = 0$ and values of U_0 obtained from the flux-creep model (Table I), as a function of δ. They behave similarly and, moreover, their absolute values almost coincide. The error bars indicate the statistical error typically involved in the determination of these quantities. Figure 10 shows directly the proportionality of $F_c(\pi/\gamma)\xi_{ab}^3$ and other energy scales with the quantity U_0. In this figure, the linear regression lines, which are constrained to pass through the origin, emphasize the linear, proportional relationship. The plot shows that $F_c(\pi/\gamma)\xi_{ab}^3$ (solid squares) is related to U_0 by a constant factor of ≈ 0.85. The similarity in the oxygen dependency of these entities is revealing and gives clear indication that the energy U_0 appearing in the interpolation formula and in the nonlinear equa-

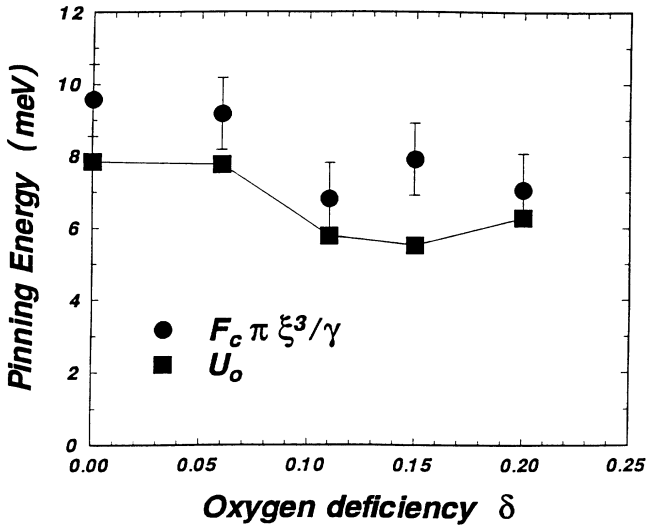

FIG. 9. The scaling energy U_0 in the nonlinear model and the product $F_c(\pi/\gamma)\xi_{ab}^3$ behave similarly as a function of the oxygen deficiency δ. Error bars show typical statistical errors. (Note that 1 meV is equivalent to an energy of 11.4 K.)

tion (13) for $U_{\text{eff}}(J,0)$ is closely associated with the vortex-pinning energy of a pointlike center.

While the interpretation up to this point is very appealing in its simplicity, there are two problems. One is that the expression used, Eq. (13) for $U(J)$, is itself a result from *collective*-pinning theory. The second problem is the field dependence of the underlying critical current density. In particular, pinning by independent pointlike defects should lead to a Kim-like dependence on the magnetic field of the form $J_c(B) \propto B_\phi/(B+B_\phi)$, where B_ϕ is related to the density and strength of pins and is written in units of flux density. The inconsistency is that the experimental results for $J_c(H)$ at low temperature are almost field independent for $H > 1$ T (see Fig. 3 in Ref. 1, for example). On the other hand, the theory for collective flux creep[14] does provide such a field independent J_c in an amorphous, one-dimensional (1D) limit.[20] This limit corresponds to a case in which the flux-line lattice parameter $a_o \approx (\phi_o/B)^{1/2}$ is larger than a transverse correlation distance R_c. For fields of 1 and 6.5 T, the intervortex spacing a_0 is $\sim$450 and 180 Å, respectively. Values for R_c can be estimated[14,20] using the relation

$$J_c = \phi_0 \xi_{ab}/(8\pi\lambda_{ab}R_c)^2 . \tag{16}$$

Inserting measured, δ-dependent values[1] for these quantities yields $R_c \approx 15$–30 Å at 4.2 K and 20–40 Å at 10 K. Hence, the condition $R_c < a_0$ clearly holds and we conclude that the 1D amorphous case is the applicable limit.

Let us now apply to the present work the results from collective flux-creep theory, noting that it provides order-of-magnitude estimates for most values. In the following, the expressions are written for the experimental case in which the magnetic field is applied along the crystalline c axis. The notation and results of Feigel'man *et al.*[14] are used. These authors consider several different current densities, of which the despairing current density j_0 is largest. It is related to the critical current density j_c in the absence of flux creep [denoted J_{c0} in Eq. (13)] by the expression $j_c \sim j_0(\xi_{ab}/L_c)^2$. We use this result to obtain values[21] for the longitudinal correlation length L_c.

Several different regimes can be encountered, depending on the relative magnitude of experimental current density j. To clarify the relative sizes of the current densities, Fig. 11 shows the various theoretical j's as a function of oxygen deficiency δ. Region A corresponds to a

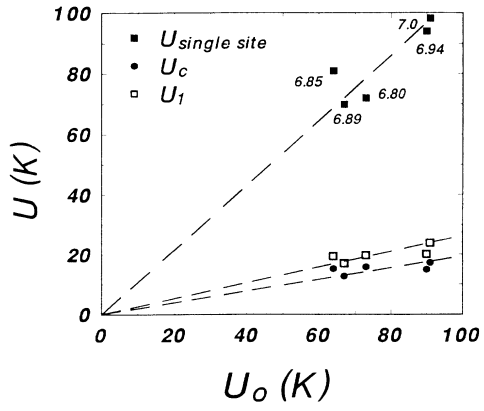

FIG. 10. A plot vs the experimental pinning energy parameter U_0 in the nonlinear function $U(J)$, Eq. (13). Various energy scales are shown: (■) the energy $F_c(\pi/\gamma)\xi_{ab}^3$ associated with a pointlike pinning center; and energies U_c (●) and U_1 (□) from collective-flux-creep theory (Ref. 16).

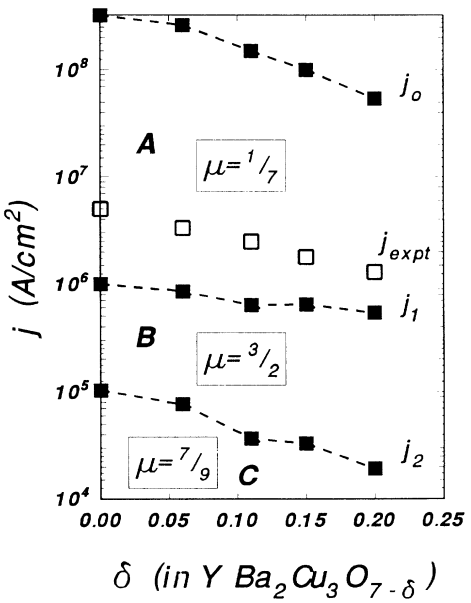

FIG. 11. Current density j for various oxygen-deficient $YBa_2Cu_3O_{7-\delta}$ materials. Shown is the depairing current density j_0, the experimentally determined current density j_{exp} and the values j_1 and j_2 from collective creep theory that define the boundaries between regions A, B, and C. Theoretical values for the exponent μ are shown.

current density $j > j_1 = j_c(L_c/a_0)^{7/5}$; in this region, the energy scale for flux motion is

$$U_c \sim [(H_c^2/8\pi)(4\pi\xi_{ab}^2\xi_c/3)](\xi_{ab}/L_c) = E_{\rm pin}(\xi_{ab}/L_c) ,$$

which has values of 13–18 K in the present study. The important exponent μ, contained in Eqs. (13) and (14), has a value of $\frac{1}{7}$. Physically, the vortex "bundle" that hops is a segment of one line with length L in the range $L_c < L < a_0$. Region B corresponds to an interval $j_1 > j > j_2 = j_1(a_0/\lambda_{ab})^2$. Here the energy scale for flux motion, $U_1 = U_c(a_0/L_c)^{1/5}$, has values of 17–24 K which are not very different from U_c. In this interval, μ has its maximum value of $\frac{3}{2}$. Physically, a small bundle of length $L \geq a_0$ and transverse extent $< \lambda_{ab}$ hops. In region C, with $j < j_2$, the energy scale is $U_2 = U_1(\lambda_{ab}/a_0)^3$; the calculated values for U_2 increase rapidly from 700 K for fully oxygenated $YBa_2Cu_3O_{7-\delta}$ with $\delta = 0$, to 3000 K for the sample with $\delta = 0.2$. Note also that U_2 increases considerably with field due to the dependence of $1/a_0^3$. The exponent μ has value $\frac{7}{9}$ in region C.

Let us now establish the region(s) to which the experiments correspond. First we recall that the flux-creep analyses gave values $\mu \approx 0.9$, which appear comparable in magnitude to the value $\frac{7}{9}$ in region C. Examination of the experimental values of current density j in Fig. 11 shows, however, that the experiments were conducted in a completely different regime. We can further rule out region C on the basis of the energy scales, since U_2 varies strongly with δ, while the experimental values for U_0 in Table I vary only modestly and nonmonotonically with δ; the magnitudes differ greatly as well, with $U_2 \gg U_0$.

Reference to Fig. 11 shows that, for all compositions, the current density lies near the boundary between region A and region B. In theory, μ switches from $\frac{1}{7}$ to $\frac{3}{2}$ at this boundary. In a real system, however, such an abrupt change seems rather unphysical. In fact, in long-term flux-creep experiments[14] on a proton-irradiated single crystal of $YBa_2Cu_3O_7$ designed to test the "interpolation formula," a smooth variation of exponent μ with temperature was observed, with limiting values that agree semiquantitatively with the theoretical predictions. Consequently, our μ values near 0.9 lie plausibly near some average of the theoretical values. These values, $\mu \approx 0.9$, also agree rather well with the values required for an optimal modeling[22] of the quasiexponential temperature dependence of $J_c(T)$ in as-prepared (unirradiated) single crystals, where values near 1.0 were obtained.

Considering now the energy scale for flux creep, we compare the magnitude and compositional dependence of the experimental quantity U_0 with energies U_c, U_1, and U_2 from collective-pinning theory. Note first that Eq. (13) for $U(J)$, which is the expression from which U_0 values were obtained, itself comes from collective-pinning theory; furthermore, the same theoretical form for $U(J)$ applies in each of the regions A, B, and C. So these energies are precisely the ones to be compared. As noted above, it turns out that $U_c \approx U_1$ for these oxygen-deficient materials, with values near 20 K and with only a weak compositional dependence. To illustrate this, the calculated U's for each sample are plotted versus the experimental U_0 values in Fig. 10. There is a clear, credible proportionality between the experimental U_0's and theoretical results for U_c and U_1, with the latter smaller by factors of ~ 5 and ~ 4, respectively. Considering the order-of-magnitude nature of the theoretical expressions, this agreement is satisfactory. It is particularly noteworthy that the energy $E_{\rm pin}$ (which is just the product of condensation energy density and a coherence volume) is a common factor in each of the theoretical energy scales, so the simple "single-site" proportionalities are actually contained within the collective-pinning analysis.

Overall, the analysis of these oxygen-deficient materials in a collective- pinning–collective-flux-creep framework gives a consistent picture to a semiquantitative level. The field independence of J_c at low temperatures points toward the 1D amorphous case and this conjecture is substantiated by estimates of the transverse correlation length R_c. Experimental values for j lie near the boundary between regions A and B, with experimental exponents μ that fall between the respective theoretical values. The calculated energy scales are consistent with this interpretation, both in magnitude and in compositional dependence. Furthermore, the present experimental values for U_0 and μ are very similar in magnitude to those used to model $J_c(T)$ in comparable single crystals.[22] From a broader perspective, the form of $U(J)$ from collective-pinning theory, Eq. (13), accurately described experimental determinations of this quantity in unirradiated and proton-irradiated $YBa_2Cu_3O_7$ crystals.[22] Furthermore, the "interpolation formula" Eq. (14) accurately described long-term studies[17] of $M(t)$ and in this work has provided self-consistent values for μ. Taken together, we believe that these features form a consistent picture of the vortex dynamics in Y-Ba-Cu-O materials at low and intermediate temperatures and give considerable experimental evidence for the collective-pinning theories.

V. SUMMARY AND CONCLUSIONS

Flux-creep measurements on a magnetically aligned polycrystalline $YBa_2Cu_3O_{7-\delta}$ sample with various oxygen deficiencies δ has shown that the normalized flux creep rate $S = d\ln M/d\ln t$ (where M is the irreversible magnetization) does not change significantly with oxygen content in the range investigated, $0 \leq \delta \leq 0.2$. Its value centers about 0.02 and its temperature dependency shows the well-known "plateau" pattern. Correspondingly, the activation energy $U_0^* = k_B T/S(T)$ of the linear Anderson-Kim model increases steadily with T for all oxygen concentrations, an unlikely situation. A more satisfactory analysis is based on the nonlinear effective potential model derived from vortex-glass and collective-pinning theories. Both lead to the "interpolation" formula for the time-dependent irreversible magnetization, which has provided an accurate description of long-term studies of magnetic relaxation. The present results lend further support to these theoretical developments since the effective potential gives a good description of the experimental data, particularly at low temperatures. At higher temperatures, the analysis becomes sensitive to the choice of the transition temperature T_x. The deduced

critical current density in the absence of flux creep, J_{c0}, decays strongly with increasing δ, as expected from pinning considerations, and is fairly well correlated with the pinning parameter $F_c(0)\xi_{ab}(0)$. The magnetic relaxation study establishes a meaningful correspondence between the experimental energy U_0 in the nonlinear $U(J)$ pinning potential and the energy scales in the collective-pinning theory. It is established that the one-dimensional, amorphous case applies to the materials in this work. Overall, the study gives further support to these recent theories for vortex motion in superconductors.

ACKNOWLEDGMENTS

We wish to acknowledge helpful discussions with L. Civale and H. R. Kerchner. J. R. T. and Y. R. S. were partially funded by the Science Alliance at the University of Tennessee, Knoxville. The research was supported by the Division of Materials Sciences, U.S. Department of Energy; technology development was funded by the U. S. Department of Energy, both under Contract No. DE-AC05-84OR21400 with Martin Marietta Energy Systems, Inc.

[1]J. G. Ossandon, J. R. Thompson, D. K. Christen, B. C. Sales, H. R. Kerchner, J. O. Thomson, Y. R. Sun, K. W. Lay, and J. E. Tkaczyk, Phys. Rev. B **45**, 12 534 (1992).

[2]J. E. Tkaczyk and K. W. Lay, J. Mater. Res. **5**, 1368 (1990).

[3]A. P. Malozemoff and Matthew P. A. Fisher, Phys. Rev. B **42**, 6784 (1990).

[4]P. W. Anderson, Phys. Rev. Lett. **9**, 309 (1962); P. W. Anderson and Y. B. Kim, Rev. Mod. Phys. **36**, 39 (1964).

[5]A. M. Campbell and J. E. Evetts, Adv. Phys. **21**, 199 (1972).

[6]C. P. Bean, Phys. Rev. Lett. **8**, 250 (1962).

[7]M. R. Beasley, R. Labusch, and W. W. Webb, Phys. Rev. **181**, 682 (1969).

[8]Y. Xu, M. Suenaga, A. R. Moodenbaugh, and D. O. Welch, Phys. Rev. B **40**, 10 882 (1989).

[9]M. P. Maley, J. O. Willis, H. Lessure, and M. E. McHenry, Phys. Rev. B **42**, 2639 (1990).

[10]J. R. Clem and V. G. Kogan, Jpn. J. Appl. Phys. **26**, 1162 (1987).

[11]M. P. Maley, P. H. Kes, G. J. Vogt, D. S. Phillips, and M. E. McHenry, Bull. Am. Phys. Soc. **36**, 984 (1991).

[12]J. R. Thompson, Y. R. Sun, D. K. Christen, H. R. Kerchner, A. P. Malozemoff, L. Civale, A. D. Marwick, L. Krusin-Elbaum, M. W. McElfresh, and F. Holtzberg, in *Physica and Materials Science of High Temperature Superconductors-II,* NATO Advanced Studies Institute Series E **209**, edited by R. Kossowsky, B. Raveau, D. Wohlleben, and S. K. Patapis (Kluwer Academic, Dordrecht, 1992), pp. 573–593.

[13]M. P. A. Fisher, Phys. Rev. Lett. **62**, 1415 (1989).

[14]M. V. Feigel'man, V. B. Geshkenbein, A. I. Larkin, and V. M. Vinokur, Phys. Rev. Lett. **63**, 2303 (1989).

[15]T. Nattermann, Phys. Rev. Lett. **64**, 2454 (1990).

[16]M. V. Feigel'man, V. B. Geshkenbein, and V. M. Vinokur, Phys. Rev. B **43**, 6263 (1991).

[17]J. R. Thompson, Y. R. Sun, and F. Holtzberg, Phys. Rev. B **44**, 458 (1991).

[18]E. Zeldov, N. M. Amer, G. Koren, A. Gupta, M. W. McElfresh, and R. J. Gambino, Appl. Phys. Lett. **56**, 680 (1990).

[19]L. Civale, A. D. Marwick, M. W. McElfresh, T. K. Worthington, A. P. Malozemoff, F. Holtzberg, J. R. Thompson, and M. A. Kirk, Phys. Rev. Lett. **65**, 1164 (1990).

[20]L. Civale, M. W. McElfresh, A. D. Marwick, T. K. Worthington, A. P. Malozemoff, F. Holtzberg, C. Feild, J. R. Thompson, D. K. Christen, and M. A. Kirk, in *Progress in High Temperature Superconductivity Vol. 31,* edited by J. L. Heiras, L. E. Sansores, and A. A. Valladares (World Scientific, Singapore, 1991), p. 25.

[21]V. M. Vinokur (private communication).

[22]J. R. Thompson, Yang Ren Sun, L. Civale, A. P. Malozemoff, M. W. McElfresh, A. D. Marwick, and F. Holtzberg, Phys. Rev. B (to be published).